SPECIAL FEATURE: PERSPECTIVE

First principles-based multiscale atomistic methods for input into first principles nonequilibrium transport across interfaces

Tao Cheng[a], Andres Jaramillo-Botero[a], Qi An[a,b], Daniil V. Ilyin[a], Saber Naserifar[a], and William A. Goddard III[a,1]

Edited by Katepalli R. Sreenivasan, New York University, New York, NY, and approved June 25, 2018 (received for review January 2, 2018)

This issue of PNAS features "nonequilibrium transport and mixing across interfaces," with several papers describing the nonequilibrium coupling of transport at interfaces, including mesoscopic and macroscopic dynamics in fluids, plasma, and other materials over scales from microscale to celestial. Most such descriptions describe the materials in terms of the density and equations of state rather than specific atomic structures and chemical processes. It is at interfacial boundaries where such atomistic information is most relevant. However, there is not yet a practical way to couple these phenomena with the atomistic description of chemistry. The starting point for including such information is the quantum mechanics (QM). However, practical QM calculations are limited to a hundred atoms for dozens of picoseconds, far from the scales required to inform the continuum level with the proper atomistic description. To bridge this enormous gap, we need to develop practical methods to extend the scale of the atomistic simulation by several orders of magnitude while retaining the level of QM accuracy in describing the chemical process. These developments would enable continuum modeling of turbulent transport at interfaces to incorporate the relevant chemistry. In this perspective, we will focus on recent progress in accomplishing these extensions in first principles-based atomistic simulations and the strategies being pursued to increase the accuracy of very large scales while dramatically decreasing the computational effort.

quantum mechanics | reactive force fields | electron force field | molecular dynamics | multiscale simulation

There has been a great deal of progress in "nonequilibrium transport and mixing across interfaces" as summarized in this issue of PNAS describing mesoscopic and macroscopic dynamics in fluids, plasmas, and other materials over scales from microscale to celestial. Such dynamical processes at the interfaces between spatial regions occupied by different matters and by matters in different physical states dominate the physical and chemical processes essential to heterogeneous catalysis, electrochemistry, semiconductor performance, and materials processing. However, to relate the continuum simulations to these essential chemical processes, we must include atomistic-scale chemical interactions and reactions, which impact the continuum-level description of nonequilibrium transport. Unfortunately, it is still challenging for experimental measurements to directly provide information about the detailed atomistic-level structures and dynamics at interfacial boundaries. Thus, quantum mechanics (QM)-based atomistic simulations offer the starting point to elucidate interfaces and their evolution under nonequilibrium conditions. However, there is a tremendous gap between practical timescales and length scales for QM (less than thousands of atoms and less than nanoseconds) and the realistic timescale and length scale for continuum descriptions of turbulent mixing at interfaces (more than micrometers and more than microseconds). Thus, the strategies for decreasing computational efforts while retaining accuracy are highly desired. Currently, a practical density functional theory (DFT) calculation, one of the most popular flavors of QM, is limited to several hundreds of atoms (10^2) for dozens of picoseconds (10^{-11} seconds). This capacity is likely to grow by an order of magnitude over the next few years, but it is still far from

[a]Materials and Process Simulation Center, California Institute of Technology, Pasadena, CA 91125; and [b]Department of Chemical and Materials Engineering, University of Nevada, Reno, NV 89557

Author contributions: W.A.G. designed research; T.C., A.J.-B., Q.A., D.V.I., and S.N. performed research; and T.C., A.J.-B., Q.A., D.V.I., S.N., and W.A.G. wrote the paper.

The authors declare no conflict of interest.

This article is a PNAS Direct Submission.

[1]To whom correspondence should be addressed. Email: wag@wag.caltech.edu.

meeting the requirement to inform the continuum degrees of freedom, which require millions of atoms (10^6) and microseconds (10^{-3} seconds). It is not so difficult to extend the scale for mechanical properties, but the problem is how to include the chemical processes important at the atomic and molecular scales while scaling to much larger systems. Successfully accomplishing this would enable first principles accuracy in the continuum modeling of transport at interfaces while including the impact of the chemistry specific to the particular materials being studied. In this perspective, we summarize the recently developed techniques for extending the capacities of QM-based atomistic simulations to bridge the gap in timescales and length scales needed to investigate turbulent mixing and interfacial transport from atomic-scale simulations. We include successful applications to indicate the current state-of-the-art simulations, which cover the topic from surface reactions to applications in advanced materials.

Extending the Length Scales and Timescales

The first step toward extending the spatial scales and timescales is to replace the Schrodinger equation of QM with atom-centered interaction potentials or force fields (FFs), which depend only on the atom positions with the electrons reduced down to an effective charge on each atom. Here, the forces are partitioned between valence interactions arising from the bond pairing of electrons and the nonbonded interactions, including electrostatic (or Coulomb) and van der Waals (vdW; attractive London dispersion plus Pauli repulsion).

Reactive FF. van Duin, Goddard, and coworkers (1, 2) developed a reactive force field (ReaxFF) that can describe reaction surfaces in such a way that bonds can form and break to describe reactions with the correct barrier heights and transition-state structures. The functional forms in ReaxFF were selected to provide accurate descriptions of bond breaking and transition states for a variety of allowed and forbidden reactions. It uses a general sigmoid-like relationship between bond order (BO) and bond distance (R_{bond}) and a relation between bond energy (BE) and BO (approximately linear) in a framework that leads to a good description of bond dissociation and transition-state energies for reactions. Other valence terms (angle and torsion) are defined in terms of BO so that all interactions go smoothly to zero as the bonds break. All parameters in ReaxFF are derived directly from QM training sets considering a large number of reactions. A well-trained ReaxFF is able to provide nearly the accuracy of ground-state QM in describing reactive processes, including barriers and rates, but at a computational cost millions of times smaller, thus making practical the molecular dynamics (MD) simulations of large-scale reactive chemical systems (millions of atoms). For example, Fig. 1 shows that ReaxFF reproduces well the four independent pyrolysis pathways of cyclotrimethylene trinitramine (RDX), an explosive with the formula $(O_2NNCH_2)_3$ (3).

Charge Equilibration with Polarization. Charge equilibration with polarization (PQEq) is a recent improvement in the description of electrostatic interactions in ReaxFF. Charge equilibration (QEq) was developed by Rappe and Goddard (4); the atomic charges on each atom are the size of an atom instead of point charges so that charges on adjacent atoms are partially shielded. QEq defines the relative charge affinity of each atom in terms of the valence averaged atomic ionization potential (IP) and electron affinity, which are combined to provide the electronegativity (χ) and hardness (J). The charges are then allowed to flow

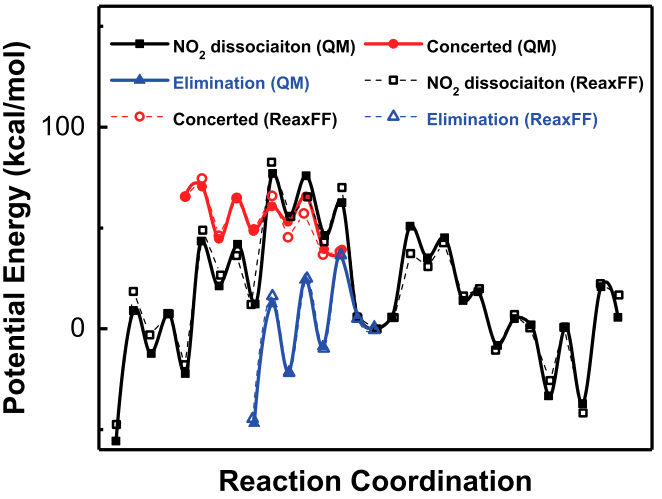

Fig. 1. Comparison of ReaxFF with QM (on the level of B3LYP/6-311G*) for decomposition of RDX molecule via all four reaction pathways (3).

dynamically at every time step of the MD, while keeping them in equilibrium (in the condition of constant chemical potential) and including the shielded interactions of charges between all centers. PQEq retains the three parameters of QEq (χ, J, and R_{atom}) but includes a fourth parameter, K, the atomic polarizability that controls magnitude in the shift of the shell charge from the nucleus (5, 6). This shell charge (with total charge e^-) is allowed to respond dynamically to the electrostatic field. PQEq improves the performance in describing the polarization response of molecules in electrostatic fields as shown in Fig. 2. PQEq exhibits much better performance than static charge models in describing polarizable system. Optimizing these four parameters involves matching to the polarization in QM as a dipole is brought along various directions to a sample set of molecules. QM-optimized PQEq parameters have been published for H, C-F, and Si-Cl (5) and for Ge-Br, Sn-I, and Pb-At (7). Generic parameters for the full periodic table (up to Z = 102, No) have been provided in the first paper (6).

Universal Nonbond Interactions. Starting with van der Waals in 1873, it has been recognized that describing the phases of matter requires an attractive interaction scaling, like $1/V^2$ (V is volume) or $1/R^6$ (R is radius), and a volume exclusion term representing the Pauli Principle (excluding pairs of electrons from overlapping) that should scale exponentially. These two-body vdW interactions are described using empirical parameters based on scattering experiments or crystal structures of molecular crystals with simple expressions, such as Lennard–Jones 12-6 or Buckingham exponential 6. An exception is the universal FF developed in the work by Rappe et al. (8), in which case nonbonded (NB) parameters were derived from atomic polarizabilities and atomic IPs. They also reported values for all atoms up to $Z = 103$.

Obviously, it would be much better to derive the NB parameters from QM. However, the Perdew–Burke–Ernzerhof (PBE) level of DFT, the only QM methodology practical for large-scale calculations, does not account for the physics of London Dispersion. For example, PBE accounts for only 8% of the heat of vaporization of crystalline benzene and leads to a volume 35% too large. A number of developments being carried out to include London Dispersion in DFT formulations; led by groups involving

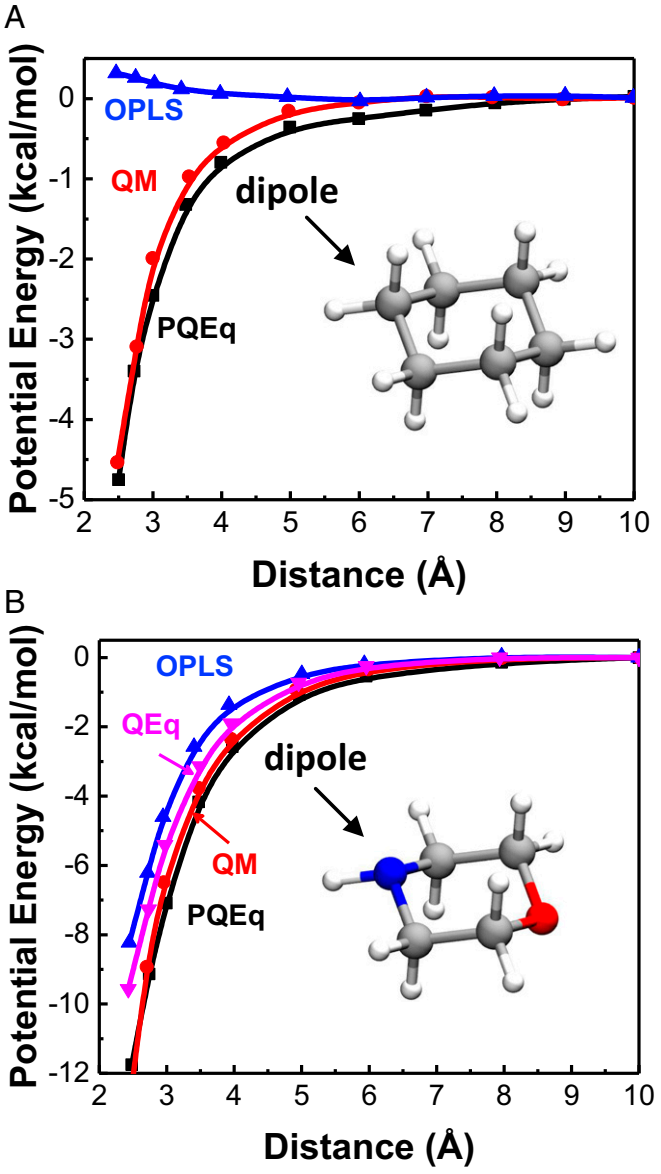

Fig. 2. QM polarization as a dipole is brought up to cyclohexane compared with PQEq, QEq, and common FFs, such as optimized potential for liquid simulations (OPLS). We see that PQEq and QEq agree well with QM, while static charge models do not.

Grimme (9), Tkatchenko and Scheffler (10), Lundqvist and coworkers (11, 12), Michaelides and coworkers (13, 14), and Xu and coworkers (3, 15). Other approaches have also been proposed (16–18). These developments of DFT calculations with London Dispersion open up the possibility of reaching experimental accuracy from ab initio calculations. The current standard for empirical corrections is the PBE with Becke–Johnson dispersion correction (PBE-D3) formulation by Grimme et al. (19) using parameters optimized by Johnson and Becke (20). Indeed, as shown in Fig. 3*A*, PBE-D3 leads to an equation of state (pressure versus density) of H_2 crystal in excellent agreement with experiment after correcting for vibrational states (phonons). We found similar results for the noble gases and for systems involving C-F and P-Cl. We found that scaling these QM NB interactions by the well depth (D_e), the equilibrium position (R_e), and the curvature (w_e) leads to nearly exactly the same two body functions for all of these elements as shown in Fig. 3*B*. Thus, it is possible to extract two body NB functions purely from QM calculations, which provide the basis for first principles-based NB terms in FF. The advantage of using this universal NB function is that it dramatically simplifies incorporating QM information into the NB interactions in a generalized way.

Polarizable Universal Nonbond ReaxFF (the New Generation of ReaxFF). Although ReaxFF has shown many successes, the optimization of the coupled nonlinear parameters makes accurate fitting to QM sometimes extremely difficult. Meanwhile, the ReaxFF parameters do not necessarily scale smoothly across the rows and columns of the periodic table, making it challenging to develop generic sets of parameters. We are now developing the next generation of ReaxFF based on the PQEq and universal NB interactions described above. The concept in this polarizable universal nonbond reactive force field (RexPoN) is to first derive PQEq and NB parameters across interaction between all atoms (including bonded atoms) and then define the valence terms to fit the best QM

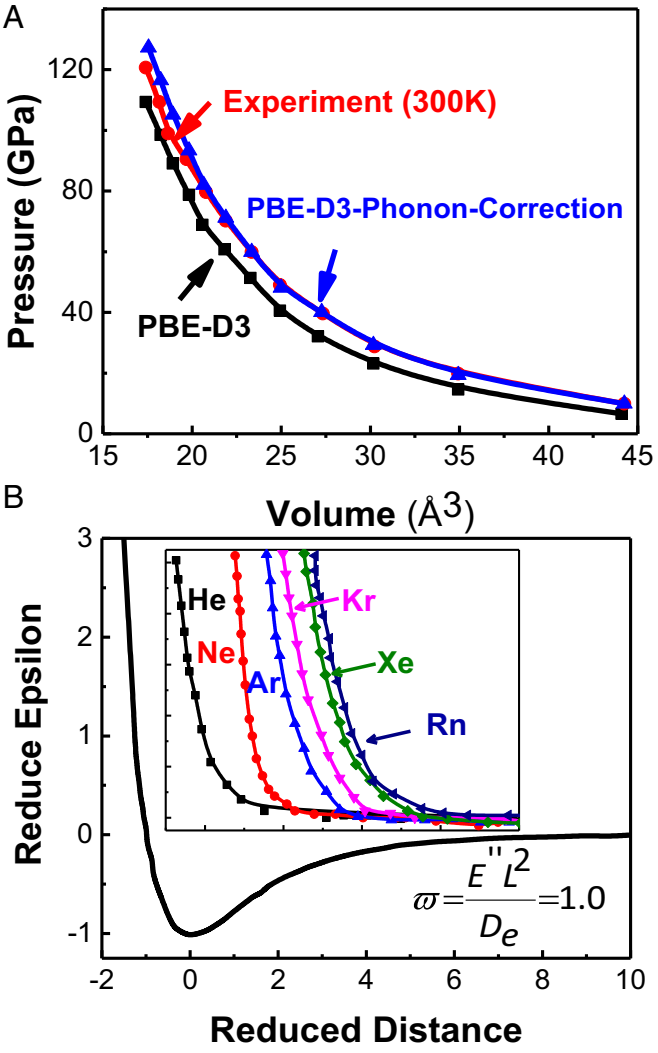

Fig. 3. (*A*) Comparison of equation of state for H_2 crystal from QM and experiment. (*B*) *Inset* shows QM-derived nonbond interactions for He, Ne, Ar, Kr, Xe, and Rn crystals. This is a demonstration that they scale to a universal NB curve (black solid curve).

description of the bonds after adding to the NB and PQEq parts. This strategy allows us to decouple NB and valence terms, which can allow for much more accurate descriptions of the bonds. For example, as shown in Fig. 4, the total polarizable reactive force field (ReaxPQ) exactly fits the exact QM O-H bond dissociation curves.

Effective Electron Methods. Highly excited heterogeneous composites are the essential elements of important processes ranging from inertial confinement fusion to semiconductor device fabrication. Understanding the dynamics of these systems is challenging, because it is difficult to extract mechanical information from experiments or theory. We developed the electron force field (eFF) approximation of QM to provide a practical way to simulate the dynamics of such systems (21–24). As in standard QM, eFF contains all electrostatic interactions between electrons and nuclei and the kinetic energy of electrons but with two approximations: (*i*) the electron orbitals are described as floating Gaussian wave packets with position and size that respond instantaneously to various forces; (*ii*) the total N-electron wave function is taken as a Hartree product with no explicit antisymmetrization. Instead, we include a spin-dependent term in the Hamiltonian that accounts for the orthogonality between same spin electrons implicit in the antisymmetrizer. This eFF framework offers the opportunity to explore and capture the dynamics of nonequilibrium phenomena that include very high energy and ionization of the electrons.

For example, in ref. 24, we used eFF to follow the effect of Auger relaxation on a diamondoid, showing that surface Auger leads to etching only of the surface carbons, whereas Auger relation of deeper atoms relaxes without etching as shown in Fig. 5. This was used to rationalize why direct current discharges with a few hundred-electronvolt electrons lead to incredibly smooth surfaces [0.25 nm for Si (100)]. Indeed, the optimum electron plasma energy for etching smooth surfaces is 200 eV for Si and SiO_2 but 500 eV for carbon and 75 eV for GPa; each is comparable with the optimum for the Auger core electron excitation. Standard QM methods cannot describe such nonequilibrium ejections of electrons or the dynamics of Auger decay. This illustrates how

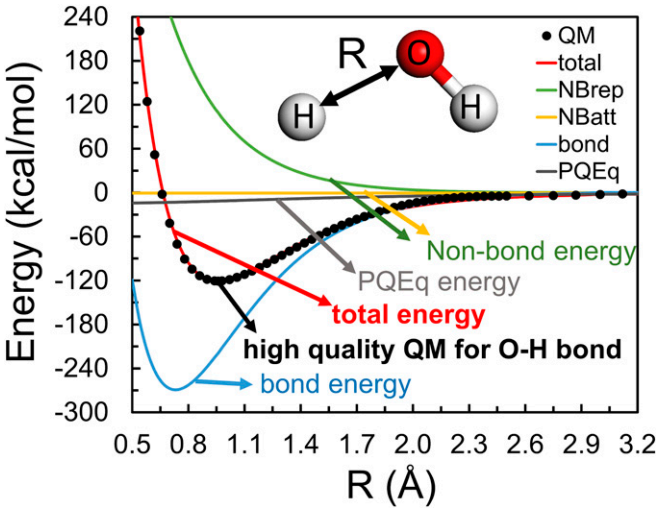

Fig. 4. Illustration of the O-H bond in water, which shows how to define the RexPoN BE that, added to the QM-based NB, exactly fits highest-level QM. NBrep, the repulsion part of nonbonded interaction; NBatt, the attractive part of nonbonded interaction.

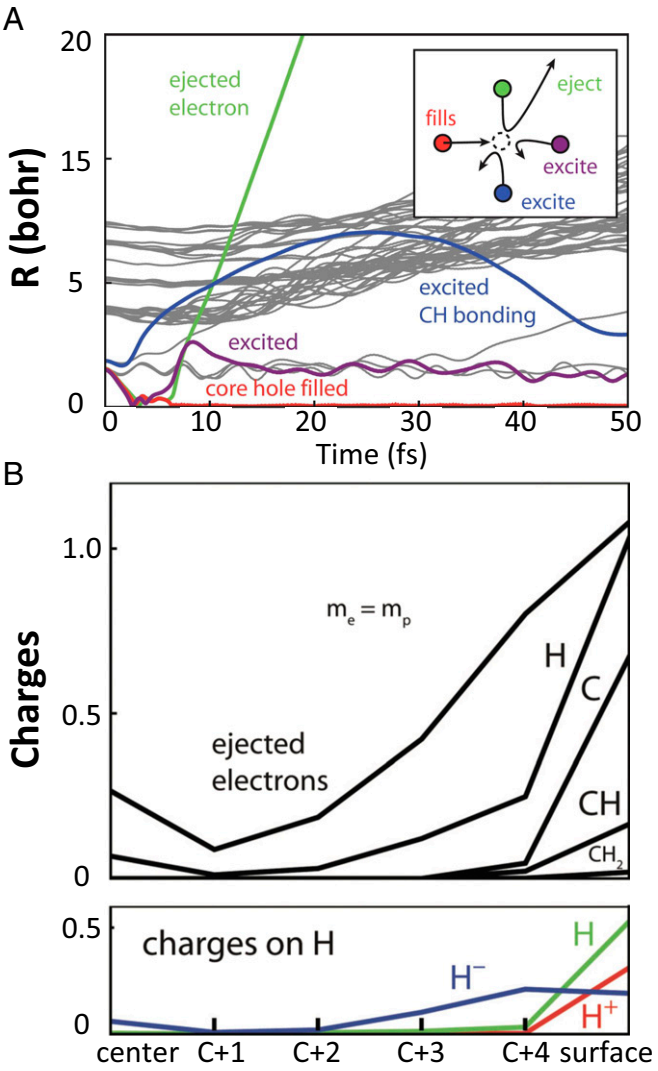

Fig. 5. Application of eFF to Auger decay-induced etching of the $C_{197}H_{112}$ diamondoid. (*A*) Distance of valence electrons from the core hole. The figure shows the green electron filling the core hole, the red electron being ejected (and trapped after 20 femtoseconds; not shown), and the blue and purple electrons being excited. *Inset* depicts color-coded trajectories of valence electrons during a core-hole filling event. (*B*) Charges-associated atomic composition of fragments separated from the nanoparticle (NP) after 50 femtoseconds.

extending the timescales and length scales of QM requires reformulations of QM.

Optimizing Parameters to Fit QM. A critical component in a first principles multiscale nonequilibrium strategy is that all FF parameters must be trained from a diverse set of QM data within a systematic optimization framework that allows methods from one scale to be parametrically tuned from those at finer scales. To this end, we developed the General Multiobjective Force Field (GARFfield) optimization framework (25). GARFfield uses a hybrid evolutionary and gradient-based scheme to enable systematic multiobjective paretooptimal optimization of electronic, atomistic (reactive and nonreactive), and coarse-grained FF parameters using QM-prepared training datasets, hence improving their accuracy and transfer ability over a broader range of compositions,

interactions, and environmental conditions unexplored by experiments. GARFfield optimization objectives include charges, cell stress, stress–strain curves, geometries, lattice parameters, heats of formation, equations of state, atomic forces, and other energy-based objectives.

Extending the Simulation Timescale

Another very important issue is extending the timescale from femtoseconds of MD to the microseconds to seconds level needed to describe the mesoscale and macroscale. Advanced sampling methods have been introduced to extend simulation timescales, such as hyperdynamics (26), replica exchange MD (27), metadynamics (28), temperature-accelerated dynamics (29), and accelerated MD methods (30). In particular, we developed the adaptive accelerated reactive force field reactive dynamics (aARRDyn) method (31) for ReaxFF by extending the bond-boost concept (32) to use BO in determining the flow of extra energy into the system. Fig. 6 shows results from a proof-of-concept application to the burning of H_2 in O_2 that considered 33 O_2 and 66 H_2 in 17 independent ReaxFF reactive dynamics. We see that, at the ignition temperature of 798 K, the time for forming one-half of the H_2O products is 538 seconds, but the computational cost is equivalent to just 1.3 nanoseconds as shown in Fig. 6.

Another direction in extending the timescale is hybridizing stochastic approaches, such as Monte Carlo (MC) with deterministic MD, which accelerates reaction steps past kinetic barriers, decreasing the number of iterations required to model state-to-state transitions in slower processes. Two commonly used MC/MD hybrid methods are grand canonical Monte Carlo/molecular dynamics (GC-MC/MD) (33) and uniform acceptance force-biased Monte Carlo/molecular dynamics (UFMC/MD) (34). The GC-MC/MD approach was initially developed to model the extent of oxidation in Pd nanoclusters (35, 36), and it is now widely used in hydrogen and carbon uptake by palladium as well as open circuit voltage profiles for Li intercalation in graphite (37) and sulfur electrodes (38) during cell discharge. The successful application of UFMC/MD simulations includes simulating the nucleation and growth of carbon nanotube (34, 39–41).

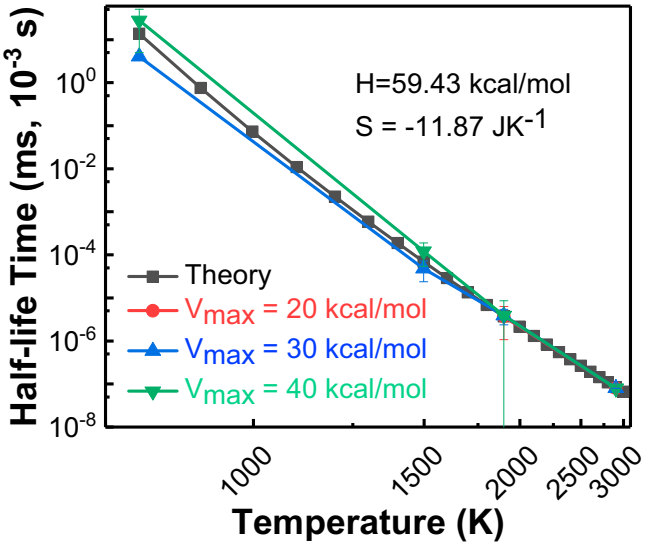

Fig. 6. The half-life time for H_2O product formation predicted from 798 K to 2,698 K using aARRDyn. The time for forming one-half the H_2O products at 798 K is 538 seconds (just 1.3 million time steps).

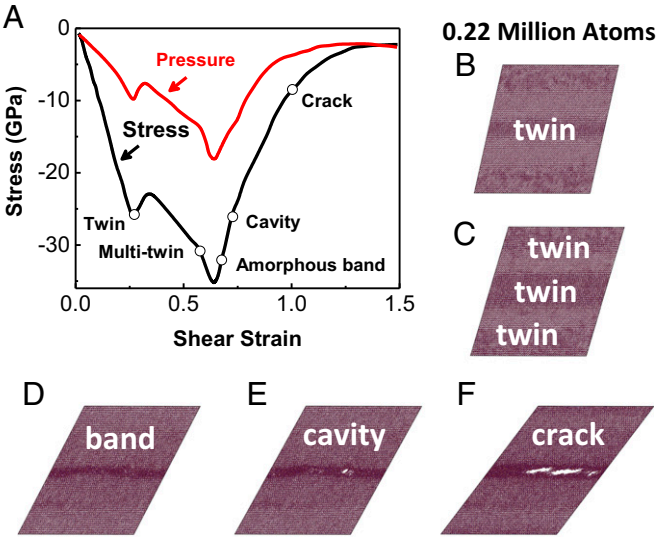

Fig. 7. Simulation of brittle fracture in B4C using the ReaxFF trained with QM. (*A*) The periodic cell has 200,000 atoms. (*B*) Stress–strain relationship as the system is sheared to brittle failure. (*C*) The successive processes of twinning, amorphous band formation, cavitation, and crack formation: (*B*) twinning initiation, (*C*) twins grow, (*D*) amorphous band initiates from twins, (*E*) cavitation within amorphous band, and (*F*) cavity grows into a crack and then massive failure.

Application of Multiscale Atomistic Methods for Interface Phenomenon

Mechanical Fracture at Interface: Origin of Brittle Fracture in Boron Carbide. Boron carbide (B4C) and related superhard materials exhibit useful properties of high melting temperature, high thermal stability, high hardness, low density, and high abrasion resistance (42, 43). However, extended engineering applications of B4C are limited by the brittle failure arising from the amorphous shear band formation (2–3 nm in width and 100–300 nm long) under high pressure (44, 45).

To determine the atomistic mechanism underlying formation of the amorphous shear band, we applied QM to determine the response to shear along 11 plausible slip systems (43). We found that the (011̄1)1101 slip system has the lowest shear strength (in agreement with experiment) and that this slip leads to a unique deformation mode before failure, in which a boron–carbon bond between neighboring icosahedral clusters breaks to form a carbon lone pair (Lewis base) on the C within the icosahedron. Additional shear then leads this Lewis base C to form a new bond with the Lewis acidic B in the middle of a CBC chain. This then initiates destruction of this icosahedron, which leads to higher density and hence, tension that induces amorphous band formation. However, to test this interpretation requires cells large enough to allow the 3-nm shear bands to be far apart, requiring a supercell (Fig. 7*A*) with at least 200,000 atoms, too large for QM.

Thus, we developed ReaxFF to accurately describe the bond-breaking process in B4C from QM simulations (42) and carried out reactive molecular dynamics (RMD) simulations on finite shear deformations of B4C at room temperature (42). We shear the system continuously until failure for two different slip systems (rhombohedral representation). We found that the deformation mechanism starts with a sequence of discrete twinning formation steps followed eventually by amorphous band formation, then cavitation, and finally, crack opening (Fig. 7). This analysis of the

failure process shows that the origin of the brittle failure fracture for B4C is the higher density of the cracked icosahedra that leads to negative pressures, which induces cavitation and eventually, crack opening. The high density of amorphous B4C was confirmed by ab initio MD simulations (42).

Chemical Reactions at the Electrolyte/Electrode Interface: Electrochemical Reduction of Carbon Dioxide on Nanocatalyst. Copper is the only elemental metal that reduces a significant fraction of carbon dioxide (CO_2) to hydrocarbons and alcohols, but the atomistic reaction mechanism that controls the product distributions was not known, because it was not been possible to detect the reaction intermediates on the electrode surface experimentally. To provide this mechanism, we used the PBE-D3 level of QM with full explicit solvent (five layers) in free energy metadynamics calculations to obtain the activation energies and onset potentials for both the 100 and 111 surfaces of Cu at pH values ranging from 0 to 7 to 14 (46–50). Amazingly, we found that the onset potentials were within 0.05 V of experiment and that the activation energies were within 0.05 eV. This validates the accuracy of the QM (46, 47, 49, 50). Because the time to equilibrate the solvent is 0.5 nanoseconds but the practical timescale of QM MD is 10 picoseconds, we used ReaxFF to relax the solvent before the QM and used advanced sampling methods to derive the free energy barriers.

Experimentally, it was found that much better performance for carbon monoxide (CO) to ethanol is obtained with 10- to 20-nm NPs of Cu grown on 9-nm carbon nanotubes using the chemical vapor deposition (CVD) experiment. These NPs contain 200,000 atoms, well outside the realm of QM. We solved this problem by using ReaxFF to simulate CVD growth of the 200,000-atom NPs, leading to grain behavior and X-ray line broadening in agreement with transmission electron microscopy (TEM) and X-ray powder diffraction (XRD). We then examined the NP and found that the undercoordinated squares sites on grain boundaries are far more active for CO reduction to ethanol than the low index surfaces (51).

Shock-Induced Formation of Hot Spots in Polymer-Energetic Materials Composites. Energetic materials are essential for applications ranging from rocket engines to building and dam construction to armaments. These energetic materials are bound together into a composite involving a matrix of polymer elastomers to form the polymer-bonded explosives (PBXs) that can be molded into various shapes while providing some control in resisting unintentional detonation due to shocks or friction. The interaction of shock waves with nonuniform interfaces plays an essential role in hot spot formation, which leads to detonation in heterogeneous PBXs as shock waves pass through the interface or other defects (52). To elucidate the origin of the hot spot formation at nonuniform interfaces, we applied ReaxFF to examine the shock passing through a realistic PBX model (PBXN-106) with a saw tooth interface (but no voids) between RDX and the polymer [hydroxyl-terminated polybutadiene (HTPB)] (52, 53) as shown in Fig. 9*A*. As the shock propagates from high-density RDX to low-density HTPB, a hot spot develops at the first asperity, where the shock wave encounters the lower-density polymer (Fig. 8*B*). This hot spot arises from adiabatic shear localization, which leads to a large temperature increase that persists long after the shock front has passed the interface. This is followed by coupling to chemical reactions (NO_2 and HONO dissociation) that ultimately lead to detonation. The hot spot formation mechanism derived from the reactive MD suggests that hot spot formation could be suppressed by decreasing the polymer density at the interface (53, 54). We tested this by examining the hot spot formation as a function of polymer densities, including the second shock, as shock waves passed through the asperity. We showed that using a much lower-density polymer (1/3 that of RDX) should dramatically decrease hot spot formation (Fig. 8*C*). This effect arises from the change in shock impedance, which decreases by approximately 51% for low density compared with increasing by 80% for high density for the shock with particle velocity of 3.5 km/s.

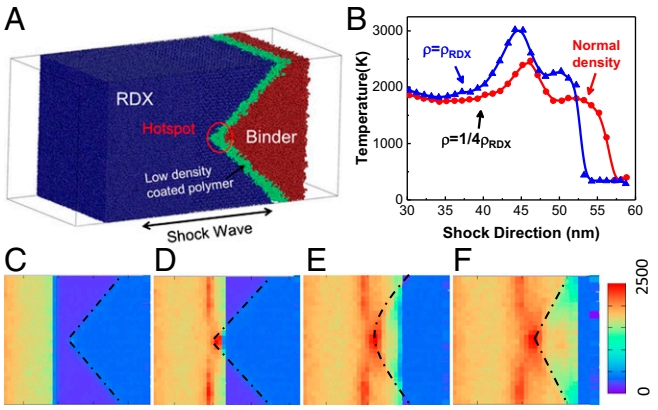

Fig. 8. Shock wave passing through a nonplanar sawtooth interface of PBX. (*A*) PBX model. (*B*) One-dimensional temperature profile at 6.5 picoseconds showing that the hot spot is suppressed by decreasing the density of the polymer. (C) Two-dimensional temperature profile showing hot spot formation at the asperity, which remains in place as the shock proceeds.

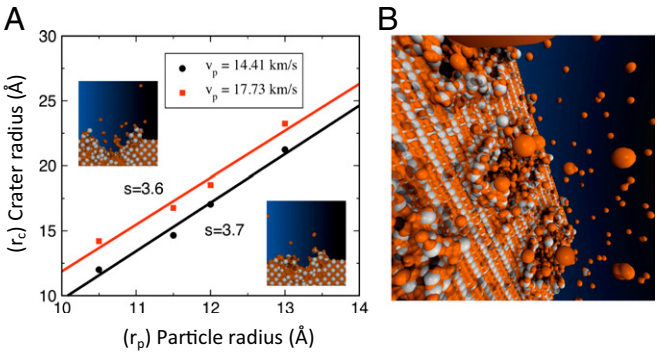

Fig. 9. (*A*) ReaxFF-simulated TiO_2 crater radius versus ice cluster impactor radius is consistent with experimental data from Kearsley et al. (56) associated with NASA's Stardust mission. Atomistic crater profiles are shown as *Insets*. The ratio of crater radius (r_c) to cluster radius (r_p) is linear over the range of impact velocities and its slope (s) provides an indication of increasing or decreasing damage [i.e., at encounter (E)5, s ¼ 3:6; therefore, larger-diameter damage is expected than at E3 with s ¼ 3:7]. Kearsley et al. (56) report s ¼ 2:2–4:63. (*B*) Sublimated titanium atoms (in orange) from INMS walls would potentially affect its accuracy in reading oxygen-containing species.

Superfast Impact and Related Reactions at Interface: The Fragmentation of Molecule-Containing Ice Particles in the Cassini–Huygens Probe of the Enceladus Moon of Saturn. The NASA/European Space Agency (ESA) Cassini probe of Saturn analyzed the molecular composition of plumes emanating from the south pole of its moon, Enceladus, and the upper

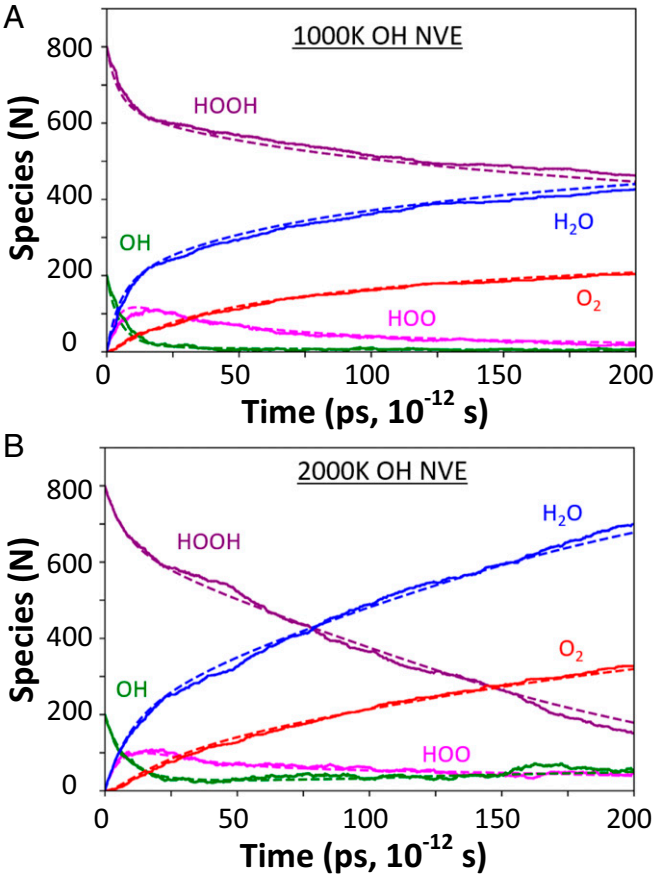

Fig. 10. Observed (solid) and analytically reproduced (dashed) number of species as a function of time for microcanonical ensemble (NVE) RMD simulation equilibrated at (*A*) 1,000 K and (*B*) 2,000 K.

atmosphere of another moon, Titan. Interpretation of these data is complicated by the hypervelocity (HV) flybys of up to 18 km/s that caused substantial molecular fragmentation within the mass spectrometer, making it very difficult to deduce the species in the original cluster. To interpret these data, we used ReaxFF to simulate the HV impact of various molecular species and ice clathrates on oxidized titanium surfaces mimicking those in Cassini's neutral and ion mass spectrometer (INMS). The predicted velocity-dependent fragmentation patterns and composition mixing ratios are consistent with those extracted from Cassini's INMS data (55), providing the means for identifying the molecules in the plume.

Our simulations also predicted that surface damage from the HV impacts on the INMS interior walls would lead to titanium metal surfaces that would serve as a sublimation pump on subsequent passes by Titan, causing confusion between N from NH_3 on Titan and hydrocarbons on Enceladus. We confirmed that this phenomenon would alter the instrument's readings due to the chemical interactions between sublimated titanium atoms and oxygen-containing species in Enceladus' plume. These results show how theory can identify chemical events from HV impacts in space plumes and atmospheres, providing in turn clues to the internal structure of the corresponding sources (e.g., Enceladus) and a valuable set of tools in steering modifications in future missions (Fig. 9).

Extracting Rate Constants for Continuum Reaction Kinetics from RMD. To illustrate how ReaxFF reactive dynamics can be applied to extract reaction mechanisms and rate constants that can be used in analytic continuum simulations of combustion, we considered the simple case of hydrogen peroxide (H_2O_2) pyrolysis to form H_2O and O_2 as final products. To speed up the process, we start with some OH radicals added to the H_2O_2 reactants and allow them to react under various temperatures and pressures, forming series of intermediates (OH and HO_2 are most prominent) to eventually produce products (H_2O and O_2). ReaxFF describes all chemical steps, allowing bond formation and dissociation with no predefined mechanism. After RMD completes, we analyze the trajectory to identify the molecules at each time step based on BOs. The reaction rate (r) can be directly drawn from RMD simulation by taking the derivatives of the concentration as a function of simulation time, which leads to the reaction rate coefficient [$k(T)$] by assuming first order on both reactants (A + B → C + D) that follows $r = k(T) \cdot [A] \cdot [B]$. It is straightforward to carry out the simulation at different temperatures (T) as shown in Fig. 10 and derive $k(T)$. From the Arrhenius equation, we derive the activation entropy (ΔS) and activation enthalpy (ΔH) from the atomistic dynamics in the condensed phase. Then using these values in analytic calculations reproduces the concentrations from the atomistic simulations.

This same procedure could be used for combustion of gasoline, diesel, or jet fuel to extract the mechanisms and rate constants for these much more complex systems. However, such analyses will need automated procedures to determine how to identify the most important intermediates and how to group together the ones with similar behavior to dampen statistical noise. It would be practical to describe a system with a million atoms and hundreds of reactions, but tackling the analysis will require development of self-correcting algorithms that use machine learning to recognize dominant reactions automatically, follow complex pathways, derive reaction mechanisms, and analyze rate constants. This could ultimately provide an unprecedented level of detail about the chemistry of complex combustion processes that might help design more efficient systems: say to minimize NOx production or soot formation.

Future Perspective. Over the next decade, we can expect advances in QM that lead to proper bond dissociation to correct spin states while properly including London Dispersion, so that we can use QM without empirical corrections to get accuracy close to the best experiments. Moreover, we can expect extensions and refinements along the lines described above of atomistic methods to the size scale of a billion atoms and timescales well beyond microseconds. We also anticipate hybrid methods with the ability to focus QM on the fine scale required for interfacial phenomena (thousands of atoms or fewer) while describing the QM seamlessly in a framework compatible with the large atomistic RexPoN, which in turn, can be smoothly described within a continuum framework extending to micrometers, seconds, and beyond. Having the macroscale informed fully by the QM would allow for accurate in silico design of materials expected to achieve unique structures and properties. Then experiments can focus on the solutions expected to be best. This should dramatically decrease the time required for new concepts on materials to be successfully incorporated into manufactured products. This will enable what Sadas Shankar of Harvard (previously responsible for theory-informed design of several generations of microelectronics) refers to as the "last mile."

Acknowledgments

The work reported here on carbon dioxide reduction was supported by the Joint Center for Artificial Photosynthesis, a US Department of Energy (DOE) Energy Innovation Hub, which is supported through Office of Science of the DOE

Award DE-SC0004993. The work on PQEq and polarizable reactive force field (ReaxPQ) was supported as part of the Computational Materials Sciences Program funded by DOE, Office of Science, Basic Energy Sciences Award DE-SC00014607 (program manager James Davenport). Other work on ReaxPQ for fuel cells was supported by National Science Foundation Grant CBET 1512759 (program manager Robert McCabe) and the new research using RexPoN is being continued with support from Office of Navel Research (N00014-18-1-2155). The computational resources are from Extreme Science and Engineering Discovery Environment, which is supported by National Science Foundation Grant ACI-1548562.

1 Chenoweth K, van Duin ACT, Goddard WA (2008) Reaxff reactive force field for molecular dynamics simulations of hydrocarbon oxidation. *J Phys Chem A* 112:1040–1053.
2 van Duin ACT, Dasgupta S, Lorant F, Goddard WA (2011) Reaxff: A reactive force field for hydrocarbons. *J Phys Chem A* 105:9396–9409.
3 Zhang IY, Xu X, Jung Y, Goddard WA (2011) A fast doubly hybrid density functional method close to chemical accuracy using a local opposite spin ansatz. *Proc Natl Acad Sci USA* 108:19896–19900.
4 Rappe AK, Goddard WA (1991) Charge equilibration for molecular dynamics simulations. *J Phys Chem* 95:3358–3363.
5 Naserifar S, Brooks DJ, Goddard WA, Cvicek V (2017) Polarizable charge equilibration model for predicting accurate electrostatic interactions in molecules and solids. *J Chem Phys* 146:124117.
6 Zhang Q, Goddard WA (2006) Charge and polarization distributions at the 90° domain wall in barium titanate ferroelectric. *Appl Phys Lett* 89:182903.
7 Oppenheim JJ, Naserifar S, Goddard WA (2018) Extension of the polarizable charge equilibration model to higher oxidation states with applications to ge, as, se, br, sn, sb, te, i, pb, bi, po, and at elements. *J Phys Chem A* 122:639–645.
8 Rappe AK, Casewit CJ, Colwel KS, Goddard WA, Skiff WM (1992) Uff, a full periodic table force field for molecular mechanics and molecular dynamics simulations. *J Am Chem Soc* 114:10024–10035.
9 Grimme S (2006) Semiempirical gga-type density functional constructed with a long-range dispersion correction. *J Comput Chem* 27:1787–1799.
10 Tkatchenko A, Scheffler M (2009) Accurate molecular van der waals interactions from ground-state electron density and free-atom reference data. *Phys Rev Lett* 102:073005.
11 Dion M, Rydberg H, Schröder E, Langreth DC, Lundqvist BI (2004) Van der waals density functional for general geometries. *Phys Rev Lett* 92:246401.
12 Lee K, Murray ED, Kong LZ, Lundqvist BI, Langreth DC (2010) Higher-accuracy van der waals density functional. *Phys Rev B* 82:081101(R).
13 Klimeš J, Bowler DR, Michaelides A (2010) Chemical accuracy for the van der waals density functional. *J Phys Condens Matter* 22:022201.
14 Klimeš J, Bowler DR, Michaelides A (2011) Van der waals density functionals applied to solids. *Phys Rev B* 83:195131.
15 Zhang Y, Xu X, William GA (2009) Doubly hybrid density functional for accurate descriptions of nonbond interactions, thermochemistry, and thermochemical kinetics. *Proc Natl Acad Sci USA* 106:4963–4968.
16 Liu Y, Goddard WA (2006) First-principles-based dispersion augmented density functional theory: From molecules to crystals. *J Chem Phys* 124:174104.
17 Kim H, Choi JM, William GA (2012) Universal correction of density functional theory to include london dispersion (up to lr, element 103). *J Phys Chem Lett* 2:360–363.
18 Román-Pérez G, Soler JM (2009) Efficient implementation of a van der waals density functional: Application to double-wall carbon nanotubes. *Phys Rev Lett* 103:096102.
19 Grimme S, Antony J, Ehrlich S, Krieg H (2010) A consistent and accurate ab initio parametrization of density functional dispersion correction (DFT-d) for the 94 elements H-Pu. *J Chem Phys* 132:154104.
20 Johnson ER, Becke AD (2006) A post-Hartree-Fock model of intermolecular interactions: Inclusion of higher-order corrections. *J Chem Phys* 124:174104.
21 Jaramillo-Botero A, Su J, Qi A, Goddard WA (2008) Large-scale, long-term nonadiabatic electron molecular dynamics for describing material properties and phenomena in extreme environments. *J Comput Chem* 32:497–512.
22 Kim H, Choi J-M, Goddard WA (2012) Universal correction of density functional theory to include london dispersion (up to lr, element 103). *J Phys Chem Lett* 2:360–363.
23 Su JT (2007) An electron force field for simulating large scale excited electron dynamics. PhD thesis (California Institute of Technology, Pasadena, CA).
24 Su JT, Goddard WA (2009) Mechanisms of auger-induced chemistry derived from wave packet dynamics. *Proc Natl Acad Sci USA* 106:1001–1005.
25 Jaramillo-Botero A, Naserifar S, Goddard WA (2014) General multiobjective force field optimization framework, with application to reactive force fields for silicon carbide. *J Chem Theor Comput* 10:1426–1439.
26 Voter AF (1997) Hyperdynamics: Accelerated molecular dynamics of infrequent events. *Phys Rev Lett* 78:3908–3911.
27 Voter AF (1998) Parallel replica method for dynamics of infrequent events. *Phys Rev B* 57:13985–13988.
28 Laio A, Parrinello M (2002) Escaping free-energy minima. *Proc Natl Acad Sci USA* 99:12562–12566.
29 Sorensen MR, Voter AF (2000) Temperature-accelerated dynamics for simulation of infrequent events. *J Chem Phys* 112:9599–9606.
30 Hamelberg D, Mongan J, McCammon JA (2004) Accelerated molecular dynamics: A promising and efficient simulation method for biomolecules. *J Chem Phys* 120:11919–11929.
31 Cheng T, Jaramillo-Botero A, Goddard WA, Sun H (2014) Adaptive accelerated reaxff reactive dynamics with validation from simulating hydrogen combustion. *J Am Chem Soc* 136:9434–9442.
32 Miron RA, Fichthorn KA (2003) Accelerated molecular dynamics with the bond-boost method. *J Chem Phys* 119:6210–6216.
33 Senftle TP, Meyer RJ, Janik MJ, van Duin ACT (2013) Development of a reaxff potential for pd/o and application to palladium oxide formation. *J Chem Phys* 139:044109–044115.
34 Neyts EC, Bogaerts A (2009) Numerical study of the size-dependent melting mechanisms of nickel nanoclusters. *J Phys Chem C* 113:2771–2776.
35 Senftle TP, Janik MJ, van Duin ACT (2014) Reaxff investigation of hydride formation in palladium nanoclusters via Monte Carlo and molecular dynamics simulations. *J Phys Chem C* 118:4967–4981.
36 Senftle TP, van Duin ACT, Janik MJ (2014) Determining in situ phases of a nanoparticle catalyst via grand canonical Monte Carlo simulations with the reaxff potential. *Catal Commun* 52:72–77.
37 Raju M, Ganesh P, Kent PRC, van Duin ACT (2015) Reactive force field study of li/c systems for electrical energy storage. *J Chem Theor Comput* 11:2156–2166.
38 Mahbubul Islam Md, et al. (2015) Reaxff molecular dynamics simulations on lithiated sulfur cathode materials. *Phys Chem Chem Phys* 17:3383–3393.
39 Neyts EC, Shibuta Y, van Duin ACT, Bogaerts A (2010) Catalyzed growth of carbon nanotube with definable chirality by hybrid molecular dynamics-force biased Monte Carlo simulations. *ACS Nano* 4:6665–6672.
40 Neyts EC, van Duin ACT, Bogaerts A (2011) Changing chirality during single-walled carbon nanotube growth: A reactive molecular dynamics/Monte Carlo study. *J Am Chem Soc* 133:17225–17231.
41 Neyts EC, van Duin ACT, Bogaerts A (2012) Insights in the plasma-assisted growth of carbon nanotubes through atomic scale simulations: Effect of electric field. *J Am Chem Soc* 134:1256–1260.
42 An Q, Goddard WA (2015) Atomistic origin of brittle failure of boron carbide from large-scale reactive dynamics simulations: Suggestions toward improved ductility. *Phys Rev Lett* 115:105501.
43 An Q, Goddard WA, Cheng T (2014) Atomistic explanation of shear-induced amorphous band formation in boron carbide. *Phys Rev Lett* 113:095501.
44 Chen M, McCauley JW, Hemker KJ (2003) Shock-induced localized amorphization in boron carbide. *Science* 299:1563–1566.
45 Reddy KM, Liu P, Hirata A, Fujita T, Chen MW (2013) Atomic structure of amorphous shear bands in boron carbide. *J Phys Chem A* 105:9396–9409.

46 Cheng T, Xiao H, Goddard WA (2015) Free-energy barriers and reaction mechanisms for the electrochemical reduction of co on the cu(100) surface, including multiple layers of explicit solvent at ph 0. *J Phys Chem Lett* 6:4767–4773.
47 Cheng T, Xiao H, Goddard WA (2016) Reaction mechanisms for the electrochemical reduction of CO_2 to CO and formate on the Cu(100) surface at 298 K from quantum mechanics free energy calculations with explicit water. *J Am Chem Soc* 138:13802–13805.
48 Xiao H, Cheng T, Goddard WA, Sundararaman R (2016) Mechanistic explanation of the ph dependence and onset potentials for hydrocarbon products from electrochemical reduction of CO on Cu (111). *J Am Chem Soc* 138:483–486.
49 Cheng T, Xiao H, Goddard WA (2017) Full atomistic reaction mechanism with kinetics for co reduction on Cu(100) from ab initio molecular dynamics free-energy calculations at 298 K. *Proc Natl Acad Sci USA* 114:1795–1800.
50 Xiao H, Cheng T, Goddard WA (2017) Atomistic mechanisms underlying selectivities in C1 and C2 products from electrochemical reduction of CO on Cu(111). *J Am Chem Soc* 139:130–136.
51 Cheng T, Xiao H, Goddard WA (2017) Nature of the active sites for CO reduction on copper nanoparticles; suggestions for optimizing performance. *J Am Chem Soc* 139:11642–11645.
52 An Q, et al. (2012) Predicted optimum composition for the glass-forming ability of bulk amorphous alloys: Application to cu–zr–al. *J Phys Chem Lett* 3:3143–3148.
53 An Q, et al. (2011) Elucidation of the dynamics for hot-spot initiation at nonuniform interfaces of highly shocked materials. *Phys Rev B* 84:220101.
54 An Q, Goddard WA, Zybin SV, Luo S-N (2014) Inhibition of hotspot formation in polymer bonded explosives using an interface matching low density polymer coating at the polymer–explosive interface. *J Phys Chem C* 118:19918–19928.
55 Jaramillo-Botero A, et al. (2012) Hypervelocity impact effect of molecules from enceladus' plume and titan's upper atmosphere on NASA's cassini spectrometer from reactive dynamics simulation. *Phys Rev Lett* 109:213201.
56 Kearsley AT, et al. (2008) Reaxff reactive force field for molecular dynamics simulations of hydrocarbon oxidationmicro-craters in aluminum foils: Implications for dust particles from comet wild 2 on nasa's stardust spacecraft. *Int J Impact Eng* 35:1616–1624.